Journal of Catalysis 284 (2011) 109–123

Contents lists available at SciVerse ScienceDirect

Journal of Catalysis

journal homepage: www.elsevier.com/locate/jcat

Sb, V, Nb containing catalysts in low temperature oxidation of methanol – The effect of preparation method on activity and selectivity

Hanna Golinska-Mazwa, Piotr Decyk, Maria Ziolek *

Adam Mickiewicz University, Faculty of Chemistry, Grunwaldzka 6, 60-780 Poznan, Poland

ARTICLE INFO

Article history:
Received 12 July 2011
Revised 8 September 2011
Accepted 8 September 2011
Available online 5 October 2011

Keywords:
Methanol oxidation
V—Sb—O oxides
Template-assisted synthesis
Nb modification
Methylal production

ABSTRACT

This study deals with the influence of preparation method of $SbVO_x$ binary oxides and modification with niobium on the catalytic properties in the oxidation of methanol. The samples were prepared in the presence of a template by two different procedures with and without the template (Pluronic 123). The template-assisted synthesis leads to higher surface area and pore volume as well as smaller size particles of different shapes than those in the materials synthesised without the template. The rutile $SbVO_4$ phase dominates in all the catalysts studied. The preparation procedure determines the formation of the additives (V_2O_5 or Sb_2O_4) and the concentration of oxovanadium species on the catalyst surface. The presence of a small amount of Sb_2O_4 acting as an electronic promoter in the oxidation of methanol is found when template-assisted synthesis is applied. Such a synthesis involves the formation of reducible oxovanadium species containing nucleophilic oxygen, playing an important role in the oxidation of methanol. Niobium loaded changes the selectivity towards DMM production. It has been found that by using different procedures of synthesis of binary $SbVO_x$ oxides and modification with niobium species, it is possible to obtain catalysts useful for the selective production of desired products (FA or MF or DMM) of methanol oxidation.

© 2011 Elsevier Inc. All rights reserved.

1. Introduction

Formaldehyde (FA), which is an important intermediate in the synthesis of many chemicals, is nowadays produced by oxidative dehydrogenation of methanol. It is commercially produced on silver and ferric molybdate catalysts [1–4]. The search for good catalysts for the selective oxidation of methanol, not only to formaldehyde (FA) but also to methyl formate (MF) and dimethoxymethane (DMM) (methylal), is still continued. Good catalysts for this reaction should contain acid-basic and redox sites [5]. The mechanism of methanol oxidation on metal oxides has been the subject of studies of many authors [e.g. 1,4–8]. In most of the considerations, it is stressed that in the first step, methoxy species are formed from methanol on acidic sites and with participation of nucleophilic oxygen (basic sites). Strong acid centres on the catalyst surface favour the dehydration of methanol to dimethyl ether. If the acid centres are of medium or weak strength, the reaction proceeds by the dehydrogenation route at which nucleophilic oxygen abstracts proton from C—H bond in methoxy species. Formaldehyde formed by this pathway is chemisorbed on the surface. The adsorbing centre must be weak enough to permit easy desorption of FA. If the active centres are stronger, FA does not desorb from the surface and interacts with the second methanol molecule towards other products: dimethyl ether (DME), methyl formate, and dimethoxymethane. The scheme of the reaction pathways proposed by Tatibouet [1] and considered by other authors [e.g. 4] is shown in Fig. 1.

Among the catalysts studied for methanol oxidation, the materials containing vanadium are of a great interest. The focus is on both vanadia supported on other metal oxides or different supports and V-containing mixed oxides materials [e.g. 7,8]. It has been shown [9] that all these materials contain surface VO_x species which are catalytically active sites for all V-containing mixed oxide catalytic materials. During the preparation of metal mixed oxides, because of rapid diffusion kinetics of VO_x, conditioned by its low Tammann temperature coupled with the low surface free energy of vanadium oxide, VO_x species are pushed to the surface of the final material [9]. The role of oxygen in the V—O-support bond in the catalytic oxidation of methanol to formaldehyde has been discussed in [7].

Recently, much effort has been made towards development of catalysts selective towards dimethoxymethane, which is a valuable product of methanol oxidation. DMM can be a potential procetane because of its high oxygen content and cetane number [10]. If DMM was used as a fuel additive, the demand for its production would increase considerably. At present DMM is recognized as environmentally friendly chemical used in pharmaceutical and perfume industries. Its traditional production is based on formaldehyde condensation with methanol over acidic catalysts such as

* Corresponding author.
E-mail address: ziolek@amu.edu.pl (M. Ziolek).

0021-9517/$ - see front matter © 2011 Elsevier Inc. All rights reserved.
doi:10.1016/j.jcat.2011.09.009

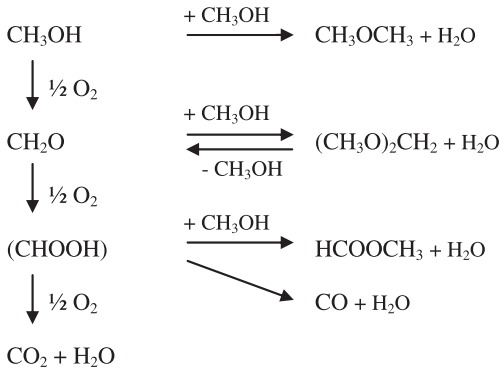

Fig. 1. The reaction pathways in methanol oxidation (according to [1]).

H_2SO_4 or $AlCl_3$ in a homogeneous system. It requires high temperatures and complicated procedure involving the risk of corrosion caused by acidic catalysts. Therefore, there is a need for one-step catalytic production of dimethoxymethane in a heterogeneous system. It is the reason why the search for catalysts for the selective oxidation of methanol to DMM has been undertaken. Recently, V_2O_5/TiO_2 [11], V_2O_5—TiO_2 sulphated [12], rhenium oxide [13], Mo-supported catalysts [14] and FeMo-based catalysts [15] have been studied for this purpose. Our study of the $SbVO_x/NbSiO_x$ system in the oxidation of methanol [16] indicated that apart from formaldehyde, DMM is also formed. Li et al. [17] used $VSbO_x/SiO_2$ for methanol selective oxidation to formaldehyde and found that Sb—V mixed oxides are more selective to formaldehyde than vanadia supported on silica because the relative amount of monomeric VO_x species is higher in mixed oxides.

In this work, our focus was on Sb and V oxides without silica, prepared by different methods and modified with niobium oxide species, as catalysts for oxidation of methanol. Our aim was (i) to prepare and characterize new $SbVO_x$ catalysts (prepared with the use of a template), (ii) to define the effect of preparation procedure on textural and catalytic properties, and (iii) to determine the role of binary oxide surface properties and niobium additives on the activity and selectivity in methanol oxidation.

2. Experimental

2.1. Preparation of samples

Two different methods were used for the production of $SbVO_x$ binary oxides. In the first (denoted **I**), $SbVO_x$ was obtained according to [18]. The procedure was as follows: 0.5849 g of NH_4VO_3 (Sigma–Aldrich) dissolved in 12 cm^3 of deionised water and 1.4944 g of $(CH_3COO)_3Sb$ (Sigma–Aldrich) dissolved in 15 cm^3 of 0.3 M tartaric acid were mixed in the flask of 100 cm^3 and evaporated at rotated vacuum evaporator (BUCHI Rotavopar RII, 100 rpm) for 10 min at room temperature and next at 353 K. The resulting solid was put into the flat dish (Ø 100 mm) and dried in oven at 353 K (heating rate 5 K/min) for 24 h, then calcined at 813 K (5 K/min) for 6 h. The amounts of precursors for V and Sb were determined to have a nominal Sb/V atomic ratio of 1.

The second method (denoted **II**) was expected to lead to mesostructured binary oxides. For this purpose, 2 g of template, Pluronic P123 ($EO_{20}PO_{70}EO_{20}$) (BASF), was dissolved in ethanol (20 cm^3) at room temperature in PP jar of 500 cm^3 and then, nitric acid (2.5 cm^3, 67%) was added to get pH ~ 6. The obtained solution is marked as **A**. Next 1.1698 g of ammonium metavanadate (Sigma–Aldrich) was dissolved in 30 cm^3 of deionised water – the solution **B**. $(CH_3COO)_3Sb$ (2.9888 g) (Sigma–Aldrich) was dissolved in 30 cm^3 of 0.3 M tartaric acid – the solution **C**. So, prepared solutions **B** and **C** were added simultaneously to the solution **A** on stirring at room temperature for 5 h. After that, the PP jar was closed and located in oven at 333 K (heating rate 1 K/min) for 48 h ageing. Next the material was filtered, transferred to a flat dish (Ø 100 mm) and dried at 333 K (heating rate 5 K/min). Afterwards, the sample was calcined at 813 K (heating rate 5 K/min) in the tube furnace in the flow of helium (40 cm^3 min^{-1}) for 6 h. The amounts of precursors for V and Sb were determined to have a nominal Sb/V atomic ratio of 1. The obtained material is labelled as $SbVO_x$(**IIa**). The **IIb** sample was prepared by the same procedure as **IIa**, the only difference was that the solutions **B** and **C** were mixed in the flask (150 cm^3) before adding to the solution **A**.

Niobium species were loaded on $SbVO_x$ supports by wet impregnation with ammonium niobiate (V) oxalate hydrate ($C_4H_4NNbO_9$) (Sigma–Aldrich) (0.0323 g dissolved in 10 cm^3 of deionised water; molar ratio Nb:Sb:V = 0.2:1:1). One gram of $SbVO_x$(IIa) or (IIb) sample located in the flask (100 cm^3) connected to the rotated vacuum evaporator (BUCHI Rotavopar RII) was evaporated for 1 h. Afterwards, the solution or niobium source was added and the wet material was rotated (100 rpm) at 353 K. After evaporation, the material was put into the flat dish (Ø 100 mm) and dried in oven at 353 K (heating rate 5 K/min) for 24 h, then calcined at 813 K (heating rate 5 K/min) in the tube furnace in the flow of helium (40 cm^3 min^{-1}) for 6 h.

2.2. Characterization of catalysts

In order to establish vanadium, antimony and niobium content ICP technique (Varian ICP-OES VISTA-MPX equipment) was applied. Prior to the analysis, 40 mg of the catalyst was mixed with excess of flux ($Li_2B_2O_7$ – about 1 g) and melt for 2 h at 1223 K in oven. The obtained colourless alloy was leached with 2 M HCl and H_2O for 4 days. The solution was analyzed by ICP.

SEM studies were conducted on a Zeiss Evo 40 operating at 17 kV. Powdered samples were deposited on a grid with a holey carbon film before transferring to electron microscope.

The prepared materials were characterized by X-ray diffraction (XRD) (AXS D8 Advance, Bruker diffractometer) with the use of Cu Kα radiation (λ = 0.154 nm) in the step scanning mode 0.05° with the 2 theta range between 10° and 60°.

The phase composition of the samples was also evaluated before and after methanol oxidation on the basis of FTIR spectra measured for a mixture of 4 mg of the catalysts and 200 mg of dehydrated KBr pressed into a pellet. Bruker Vector 22 FT-IR spectrometer (resolution 4 cm^{-1}) was applied.

The surface area and pore volume of the catalysts were estimated by nitrogen adsorption at 77 K using the conventional technique on a Micromeritics 2010 apparatus. Prior to the adsorption measurements, the samples were degassed in vacuum at 573 K for 2 h.

UV–Vis spectra were recorded on a Varian-Cary 300 Scan UV–visible spectrophotometer with an integrated sphere CA-30I. Catalysts, dehydrated at 673 K for 2 h, in the form of powders were placed into a cell equipped with a quartz window. The Kubelka–Munk function (F(R)) was used to convert reflectance measurements into equivalent absorption spectra using the reflectance of SPECTRALON as a reference.

The electron spin resonance (ESR) study was performed at 77 K and room temperature (RT) using RADIOPAN SE/X 2547 spectrometer. A cavity operating at a frequency of 8.9 GHz (X-band) with 100-kHz field modulation was used. The spectra were recorded for fresh samples and catalysts evacuated at various temperatures. Moreover, changes in the spectra after oxygen admission were analyzed, and the spent catalysts (after oxidation of methanol) were studied.

Photoemission spectra (XPS) were collected by a VSW Scientific Instrument spectrometer, equipped with a standard Al Kα excitation source. Peak intensities were estimated by calculating the integral of each peak after smoothing and subtraction of the Shirley-shaped background, then fitting the experimental curve by a least-squares routine supplied by the instrument manufacturer using Gaussian and Lorentzian lines. Atomic ratios were computed from the intensity ratios normalized by atomic sensitivity factors. The binding energy (BE) reference was taken at the C 1s peak from carbon contamination of the samples at 284.6 eV. An estimated error of ±0.1 eV can be assumed for all measurements.

Surface properties of the materials prepared were studied by in situ FT-IR spectroscopy of pyridine adsorbed. Self-supporting pellets of around 10 mg cm^{-2} were prepared and located in a classical glass cell connected to a vacuum-adsorption apparatus for in situ experiments. IR spectra were recorded at room temperature with a Bruker Vector 22 FT-IR spectrometer (resolution 4 cm^{-1}). All the samples were activated in situ at 673 K for 3 h under vacuum before adsorption of pyridine. Pyridine (Sigma–Aldrich) was adsorbed at 373 K and evacuated at different temperatures (373–523 K) for 30 min at each temperature. The IR spectra of the activated samples were subtracted from those recorded after the adsorption of pyridine. The reported spectra are the results of this subtraction.

2.3. Activity measurements

The catalysts were pressed (~20 MPa) and granulated to 0.5 < Ø < 1 mm size fraction before each test reaction.

2.3.1. Acetonylacetone cyclization – test reaction

The catalysts were tested in acetonylacetone (AcOAc) cyclization as the probe reaction. A tubular, down-flow reactor (Ø 8 mm; length 80 mm) was used for AcOAc cyclization reaction that was carried out at atmospheric pressure, using nitrogen as the carrier gas. The catalyst bed (0.1 g, 2 mm height in the reactor) was first activated for 2 h at 673 K (heating rate 15 K/min) under nitrogen flow (40 cm^3 min^{-1}). Subsequently, a 0.5 cm^3 of acetonylacetone (Fluka, GC grade) was passed continuously into the catalyst at 623 K. The substrate was delivered with a pump system (KD Scientific) and vaporized before being passed through the catalyst with the flow of nitrogen carrier gas (40 cm^3 min^{-1}). The reaction products were collected for 30 min downstream of the reactor in a cold trap (liquid nitrogen + 2-propanol) and analyzed by gas chromatography (SRI 310 C, MXT®-1 column 30 m, temperature of column 373 K) with TCD detector. Helium was applied as a carrier gas.

2.3.2. 2-propanol decomposition – test reaction

The 2-propanol dehydration and dehydrogenation was performed using a microcatalytic pulse reactor (Ø 6 mm; length 80 mm) inserted between the sample inlet and the column of a CHROM-5 chromatograph. A portion of 0.1 g (3 mm height in the reactor) of granulated catalyst was activated at 673 K (heating rate 10 K/min) for 2 h under helium flow (40 cm^3 min^{-1}). The 2-propanol (Chempur Poland) conversion was studied at various temperatures using 3-μl pulses of alcohol under helium flow (40 cm^3 min^{-1}). The substrate was vaporized before being passed through the catalyst bed with the flow of helium carrier gas. The products such as propene, 2-propanone (acetone) and diisopropyl ether were identified by CHROM-5 gas chromatograph online with microreactor. The reaction mixture was separated on a 2-m column filled with Carbowax 400 loaded on Chromosorb W (80–100 mesh) at 338 K in helium flow (40 cm^3 min^{-1}) and detected by TCD.

2.3.3. Methanol oxidation in gas phase

The methanol oxidation reaction was performed in a fixed-bed flow reactor (Ø 5 mm; length 70 mm). A portion of 0.1 g of the pure (not diluted) catalyst of the size fraction of 0.5 < Ø < 1 mm was placed in the reactor (4 mm height in the reactor). The samples were activated in argon flow (40 cm^3 min^{-1}) at 673 K for 2 h (the rate of heating was 15 K/min). Then, the temperature was decreased to that of the reaction. The reactant mixture of Ar/O_2/MeOH (88/8/4 mol%) was supplied at the rate of 40 cm^3 min^{-1} for standard reactions. Methanol (Chempur Poland) was introduced to the flow reactor by bubbling argon gas through a glass saturator filled with methanol. The typical reactions were conducted at GHSV = 80,000 h^{-1} g^{-1}_{cat}. Moreover, for a selected catalyst, the reactions under different methanol and oxygen compositions were performed. They were as follows: Ar/O_2/MeOH (88/4/8 mol%) with O_2/MeOH molar ratio of 0.5 and Ar/O_2/MeOH (92/4/4 mol%) with O_2/MeOH molar ratio = 1. The total flow rate, 40 cm^3 min^{-1}, was the same for all experiments. The reactor effluent was analyzed using an online two gas chromatographs. One chromatograph GC 8000 Top equipped with a capillary column of DB-1 operated at 313 K – FID detector was applied for analyses of organic compounds and the second GC containing Porapak Q and 5A molecular sieves columns for analyses of O_2, CO_2, CO, H_2O and CH_3OH – TCD detector. The columns in the second chromatograph with TCD were heated according to the following programme: 5 min at 358 K, increase of the temperature to 408 K (heating rate 5 K/min), 4 min at 408 K, cooling down to 358 K (for the automatic injection on the column with 5A), 10 min at 358 K, increase of the temperature to 408 K (heating rate 10 K/min), 11 min at 408 K. Argon was applied as a carrier gas. The outlet stream line from the reactor to the gas chromatograph was heated at about 373 K to avoid condensation of reaction products.

3. Results

3.1. Characterization

3.1.1. SEM images

The morphology of binary $SbVO_x$ oxides was verified by SEM images (Fig. 2). There is no doubt that the procedure of synthesis determines the size and shape of particles. The sample prepared without the template exhibits larger and oval-shaped particles. SEM images in different scales allow us to differentiate between the shape of particles of $SbVO_x$(IIa) and $SbVO_x$(IIb) – both prepared by template-assisted method. It is also important to stress the presence of additional phases visible when 1 μm scale is applied.

3.1.2. N_2 adsorption isotherms and XRD

Textural parameters and chemical composition of all the samples used are summarized in Table 1. The surface area of all the $SbVO_x$ samples was higher than that typically reported for rutile-type mixed oxides prepared with conventional methodologies like the slurry-redox, leading to surface areas lower than 10 m^2/g. The BET surface area of the catalysts prepared by method II (with the template) is higher than that of the sample prepared by method I (without the template). It is clear that the synthesis with the use of template gives higher surface area and pore volume and also smaller crystallite sizes. After modification with niobium species, the surface area of all $SbVO_x$ samples decreases.

The N_2 adsorption/desorption isotherms of $SbVO_x$ samples are shown in Fig. 3. The isotherms of both materials prepared with the use of template are of type IV, according to the IUPAC classification. They are typical of mesoporous materials and exhibit the inflection point and hysteresis loop at p/p_0 at ~0.8–0.9. It is not the case for the sample synthesized by method I. The main difference in the porosity

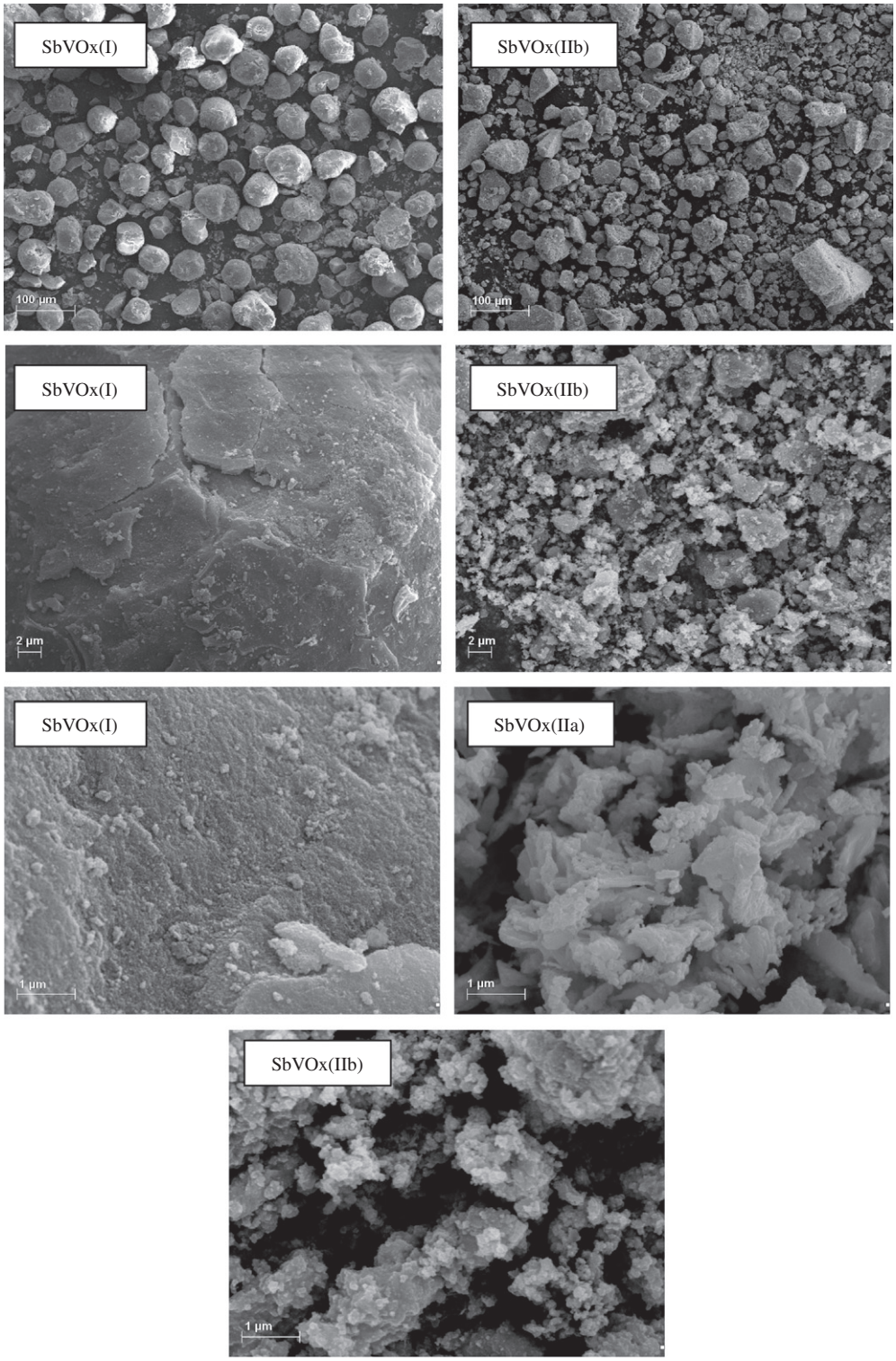

Fig. 2. SEM images (at different scales) of antimony–vanadium oxides.

of both samples prepared according to the same procedure II, but using the different system of metal sources admission to the template solution, is in the total pore volume (higher for the $SbVO_x$(IIa)) and the character of pore size distribution (PSD) (Fig. 4). A wider PSD is seen for $SbVO_x$(IIa), and this sample contains also very small mesopores of ca 2.5 nm, not found in $SbVO_x$(IIb).

The XRD patterns of all $SbVO_x$ show well visible forms of crystalline bimetallic oxides, $SbVO_4$, which could be assigned to rutile $Sb_{0.95}V_{0.95}O_4$ (JCPDS 16-0600) structure. The XRD patterns in Fig. 5 clearly show the domination of rutile $Sb_{0.95}V_{0.95}O_4$ structure. The samples prepared with the template exhibit additional peaks at 2 theta = 29.3 and 30.5°, which can be assigned to Sb_2O_4 phase described in literature [19]. The peaks are sharper in the pattern of $SbVO_x$(IIb) sample than in that of $SbVO_x$(IIa), suggesting a better dispersion of Sb_2O_4 phase on $SbVO_x$(IIa). This phase is not observed in the XRD pattern of $SbVO_x$(I), where the other peaks, besides those of rutile phase, are present. They are assigned to vanadium oxide crystalline phase (JCPDS 01-0359).

Table 1
Texture/structure parameters and chemical composition.

Catalyst	Surf. area BET (m^2/g)	Pore volume BJH (cm^3/g)	$Sb_{0.95}V_{0.95}O_4$ size (XRD) (nm)		% wt. of Sb	% wt. of V	% wt. of Nb
			2Θ = 27.4 (110)	2Θ = 53.4 (211)			
$SbVO_x$(I)	13	0.004	34	31	48.6	19.6	–
$SbVO_x$(IIa)	21	0.08	26	17.7	45.9	18.5	–
$SbVO_x$(IIb)	17	0.05	28.6	17.5	50.9	17.1	–
Nb/$SbVO_x$(IIa)	9	0.03	–	–	44.3	18.0	6.8
Nb/$SbVO_x$(IIb)	13	0.06	–	–	49.7	16.9	7.6

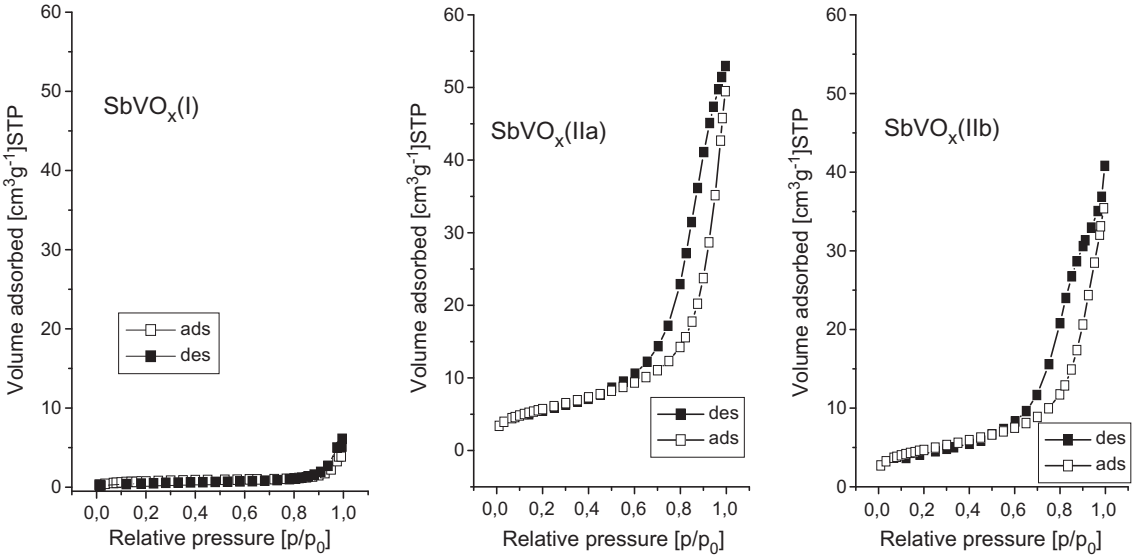

Fig. 3. N_2 adsorption/desorption isotherms for antimony–vanadium oxides.

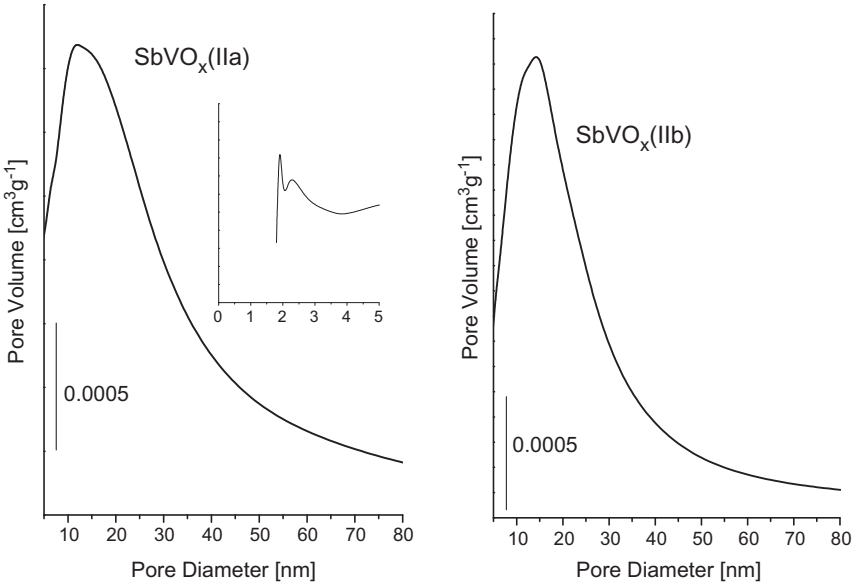

Fig. 4. Pore size distribution depending on the preparation procedure.

The $SbVO_x$ sample (IIa) modified with niobium species includes the Nb_2O_5 phase deduced form the peaks at the same positions as those assigned to Nb_2O_5 in the catalogue (Fig. 5i – JCPDS 19-0864). However, not all peaks assigned to Nb_2O_5 are present in both XRD patterns (Fig. 5g and h), suggesting some distortion of this phase or mixing of different niobium oxide structures. The reflex at 14° characteristic of Nb_2O_5 is present only in the pattern of $SbVO_x$(IIa). Interestingly, this observation indicates that a slight change in the preparation procedure of the support (methods IIa *vs* IIb) results in a significant change in the texture of niobia phase loaded.

Table 1 reveals two values of particle size of $SbVO_x$ supports calculated from two different XRD peaks. Depending on the prepara-

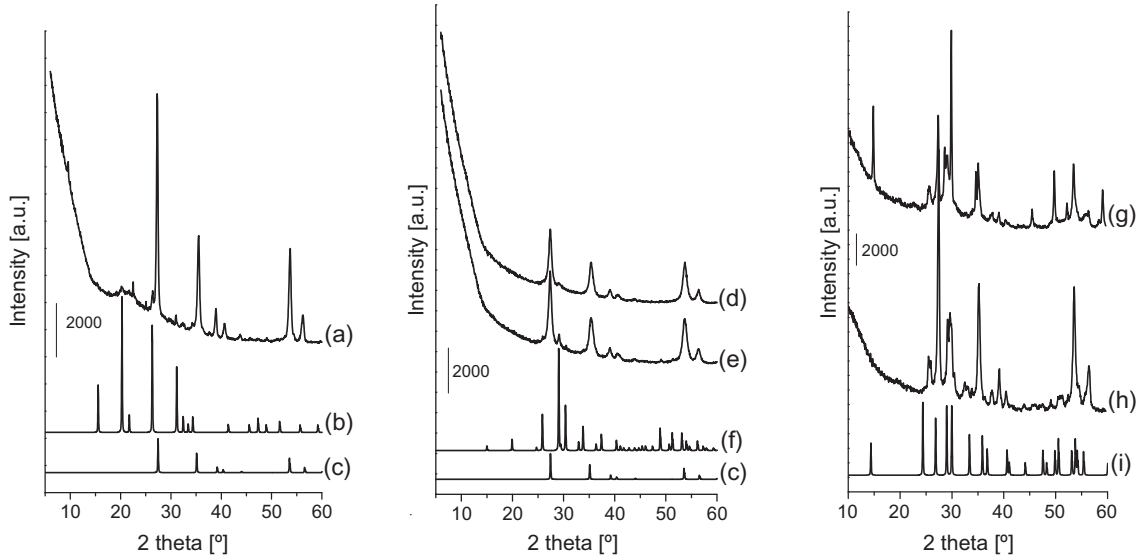

Fig. 5. The XRD patterns of: (a) $SbVO_x$(I); (b) V_2O_5 (JCPDS 01-0359); (c) $Sb_{0.95}V_{0.95}O_4$ (JCPDS 16-0600); (d) $SbVO_x$(IIa); (e) $SbVO_x$(IIb); (f) Sb_2O_4 (JCPDS 11-0694); (g) Nb/$SbVO_x$(IIa); (h) Nb/$SbVO_x$(IIb); (i) Nb_2O_5 (JCPDS 19-0864).

tion procedure of $SbVO_x$, different particle sizes were obtained. Method I leads to bigger particles than method II. There is no considerable difference in the $SbVO_x$ crystallite size between the samples prepared according to methods IIa and IIb. The type of preparation method determines also the phase composition of surface species, which is documented below.

3.1.3. Ultraviolet–visible spectroscopy

UV–vis region examined is associated with the transfer of electron from oxygen to the transition metal. For all catalysts, low energy charge transfer, LCT, characteristic of the charge transfer between vanadium and oxygen, can be observed in the 200–500 nm region. It is characteristic of V^{5+} cationic species [20]. The contribution from d–d transition of V^{4+} (d^1) that gives a broad band in the 550–800 nm region [20,21] is observed for the catalyst prepared by method IIa (a shoulder at ca 570 nm – Fig. 6a and e). The UV–vis band at ca 362 nm is very intense as typical of rutile structure of binary oxide, $Sb_{0.95}V_{0.95}O_4$. Unfortunately, UV–vis spectra do not allow us to distinguish the niobium, vanadium–antimony phases. The octahedral coordinated niobium species give a characteristic absorption band at ca. 330 nm according to [22,23], and if such a band exists in the spectrum of the sample examined, it is covered by a broad one originating from vanadium species. In niobium impregnated samples, the UV–vis bands from Nb_2O_5 and $SbVO_4$ can be located at the same position and therefore, these species cannot be distinguished on the basis of these spectra. Literature [24] describes different antimony oxides, giving rise to the bands at the same region: assigned to Sb^{3+} (195–230 nm), Sb^{4+} and $Sb^{4.33+}$ (230–280 nm and 480 nm) and Sb^{5+} (300–340 nm). The UV–vis spectrum of $SbVO_x$(I) suggests the presence of V_2O_5 phase deduced from the similar shape of UV–vis spectra for both materials (Fig. 6c and d) – especially characteristic is the band at 262 nm.

3.1.4. Infrared spectroscopy

To identify the metal species present in the samples, FTIR spectra were measured (Fig. 7). They show bands typical of binary oxide materials. On the basis of literature [e.g. 25], the IR bands below 800 cm^{-1}, e.g. at 540, 665, 735 cm^{-1} for $SbVO_x$(IIa), can be assigned to typical $SbVO_4$ rutile phase. V=O vibrations give rise to the IR bands at ~1080 cm^{-1} (trimer) and 1007 cm^{-1} (monomer) [26,27], whereas α-Sb_2O_4 is characterized by a band at ca 450 cm^{-1} [28]. This band at 450 cm^{-1} originating from α-Sb_2O_4 is present only in the spectra of the materials prepared according to procedure II (with the use of the template) in agreement with the results obtained from XRD. The bands at 826, 861 cm^{-1} can be assigned to the V—O—V vibration [29]. It is also possible to relate the bands at 1007 and 860 cm^{-1} to the cation vacancies present in rutile $Sb_{0.9}V_{0.9+x}\square_{0.2-x}O_4$ [25]. These bands are not present in the spectra of $SbVO_x$(I) and $SbVO_x$(IIb). The intensity ratios of these two bands (1007 and 860 cm^{-1}) related to those at 540 cm^{-1} are proportional to the number of vacancies per unit cell. Interestingly, niobium loading on $SbVO_x$ leads to a decrease in the intensity of the band at ca 540 cm^{-1} characteristic of Sb—O—V vibration and causes a shift in its position to 551 cm^{-1}. Moreover, it shifts the position of bands assigned to V—O—V vibration (to 827 and 866 cm^{-1}), showing that the niobium loaded interacts with vanadium species and niobium oxide is located near cation vacancies. The intensity ratio (1007/551 cm^{-1}) increases after niobium loading, suggesting formation of additional defect holes (cation vacancies). It is worth stressing the presence of an intense band at ca 740 cm^{-1} for $SbVO_x$(I) and $SbVO_x$(IIb) originating from Sb_2O_3/Sb_2O_5 [28].

The FT-IR results clearly show that the differences in phase composition of $SbVO_x$ materials depend on the preparation procedure.

3.1.5. Electron paramagnetic resonance study

The complementary information was obtained from paramagnetic electron resonance study. Generally, various vanadium(IV) species can be detected by the ESR technique. V(IV) clusters lead to a broad signal reflecting significant dipolar interactions found, e.g. in VMCM-41 samples with a high vanadium content, to which vanadium was introduced in one pot synthesis [30,31]. The spectra of the isolated V(IV) species, mainly oxovanadium VO^{2+} ions, exhibit a hyperfine structure (ESR signal splits eightfold) derived from the interaction of free electrons ($3d^1$) with the magnetic nuclear moment of V ($I - 7/2$). The bulk compound of the rutile structure ($Sb^{5+}_{0.92}V^{4+}_{0.8}V^{3+}_{0.1}\square_{0.2}O_4$) and nearly stoichiometric composition $Sb^{5+}V^{4+}O_{4.5}$ exhibits also the presence of isolated VO^{2+} ions besides dimeric species [32,33]. The ESR spectra obtained within this work are shown in Fig. 8. The difference between the spectra of $SbVO_x$(-IIa) and (IIb) is notable. Both exhibit hyperfine structure typical of

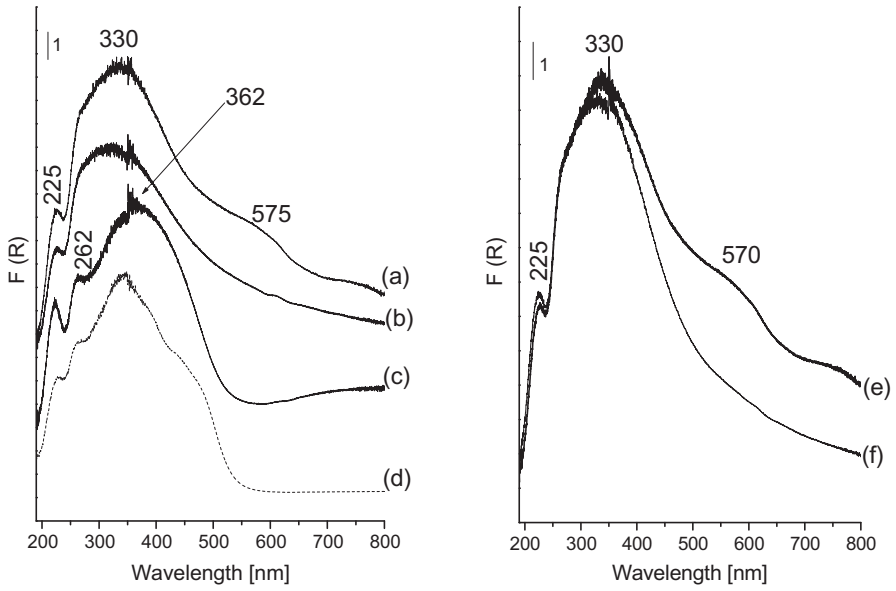

Fig. 6. UV–Vis spectra of: (a) $SbVO_x$(IIa); (b) $SbVO_x$(IIb); (c) $SbVO_x$(I); (d) V_2O_5; (e) $Nb/SbVO_x$(IIa); (f) $Nb/SbVO_x$(IIb).

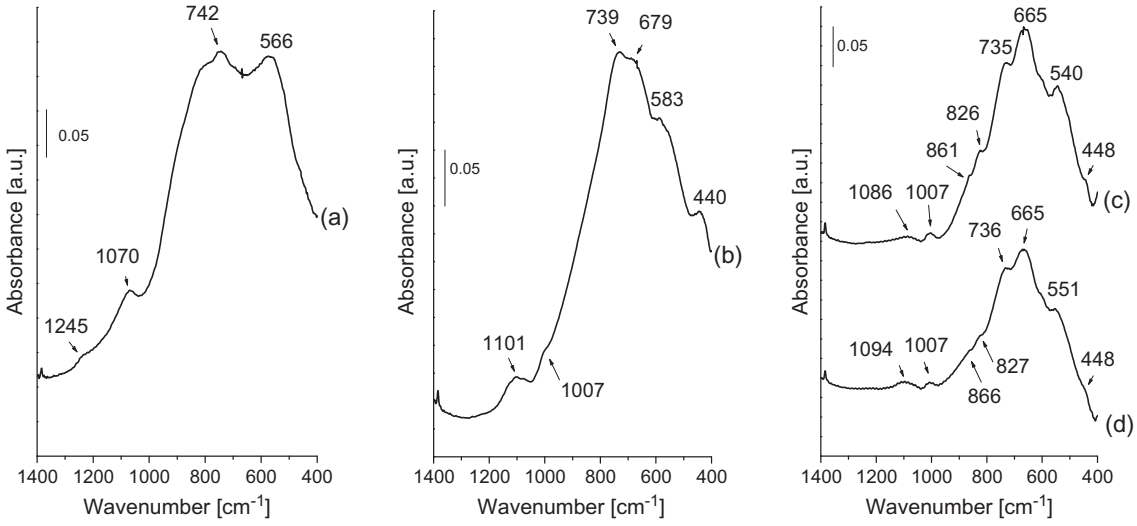

Fig. 7. FTIR spectra in the skeleton region of: (a) $SbVO_x$(I); (b) $SbVO_x$(IIb); (c) $SbVO_x$(IIa); (d) $NbSbVO_x$(IIa).

VO^{2+}, but in $SbVO_x$(IIa) V^{4+} species additionally interact with one another as can be deduced from the broadening of the ESR line. The g value (1.9665) and a shape of this line are characteristics for VO^{2+} dimmers [34]. The spin Hamiltonian parameters for $SbVO_x$ samples are presented in Table 2. Interestingly, the impregnation with niobium species diminishes the hyperfine structure of the band assigned to VO^{2+}, suggesting the chemical interaction between oxovanadium VO^{2+} species and the niobium loaded (Fig. 8B). This suggestion was confirmed by the XPS study described below. The ESR spectrum of $SbVO_x$(I) sample (Fig. 8A) indicates the well-resolved hyperfine structure originating from V^{4+} paramagnetic species. [35,36]. It is important to stress that the hyperfine structure of the spectrum of $SbVO_x$(I) is present also for the sample exposed to air at room temperature (Fig. 8C), not only after evacuation at RT.

The difference in V^{4+} species for $SbVO_x$ samples (I) and (IIa)–(IIb) is not only in the A_{iso} and g_{iso} calculated according to [35] (Table 2) but also in their stability under vacuum and oxygen treatment at different temperatures. The data in Table 2 indicate the presence of isolated vanadyl species with different symmetries like square pyramidal and octahedral, presenting different distortion. All the isolated species observed for $SbVO_x$ catalysts have been characterized by average values of g_{iso} and A_{iso} ($g_{iso} = (g_{II} + 2\,g_{\perp})/3$; $A_{iso} = (A_{II} + 2A_{\perp})/3$). The values shown in Table 2 related to those published in the work [35] and presented in a diagram of Davidson and Che allow us to state that $SbVO_x$(I) has the lowest value of A_{iso} which indicates a partial attenuation of the vanadyl character in comparison with the species on $SbVO_x$(IIa) and $SbVO_x$(IIb). Moreover, vanadyl groups for $SbVO_x$(I) are likely to be more coordinatively saturated, which makes them better resistant to the reduction and oxidation in contrast to $SbVO_x$(IIa) and $SbVO_x$(IIb) materials. The values of A_{iso} and g_{iso} for the latter two materials suggest that the ESR signals may be derived from a 5 coordinated vanadyl group having a distorted octahedral structure and one coordination vacancy in the equatorial plane [35].

It is clear from Fig. 9 that vanadium + 4 is oxidized under oxygen atmosphere much easier on $SbVO_x$(IIa) than on $SbVO_x$(I). The temperature stability of V^{4+} under vacuum treatment is also higher

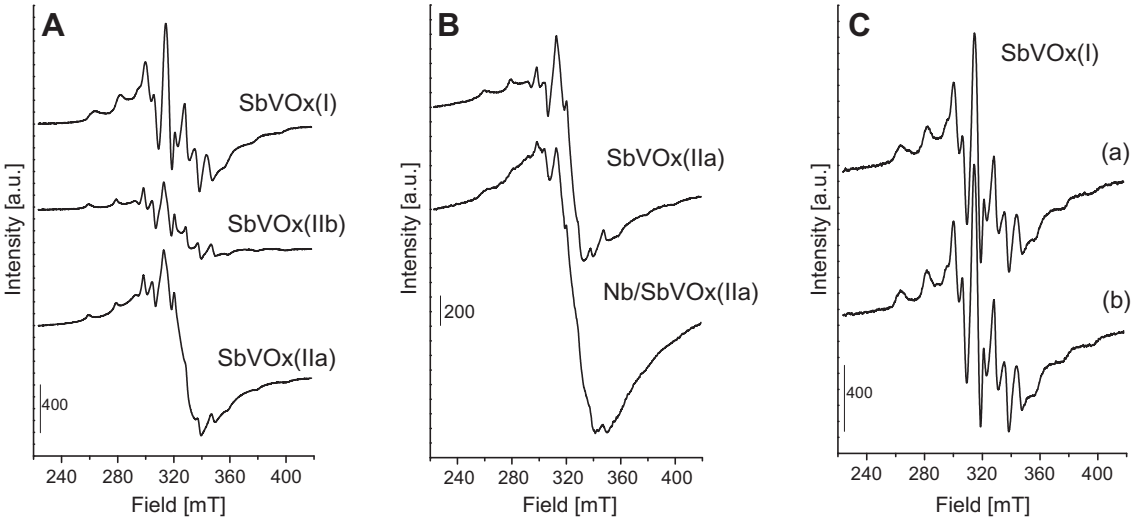

Fig. 8. ESR spectra: (A) recorded at 77 K; the samples were evacuated for 5 min at RT before scanning the spectra. $SbVO_x$(I) (gain 2.5 times higher); (B) recorded at RT of $SbVO_x$(IIa) before and after niobium loading; (C) recorded at RT (a) fresh sample in contact with air; (b) fresh sample after connection to a vacuum line and short evacuation.

Table 2
Spin Hamiltonian parameters of isolated V^{4+} species.

Catalyst	g_{II}	$g_{\perp}$	g_{iso}	A_{II} (G)	$A_{\perp}$ (G)	A_{iso} (G)
$SbVO_x$(I)	1.9313	1.9885	1.9693	188.5	69.7	109.3
$SbVO_x$(IIa)	1.9296	1.9852	1.9667	203.3	78.7	120.2
$SbVO_x$(IIb)	1.9324	1.9846	1.9672	203.4	78.4	120.1

in $SbVO_x$(I) as evidenced from Fig. 10. Evacuation of $SbVO_x$(IIa) at 373 K causes the disappearance of the hyperfine structure of the signal assigned to VO^{2+} isolated species. The lower stability of vanadium oxidation state on the catalyst surface can be attractive in oxidation processes where easy changes in metal charge are very important.

3.1.6. X-ray photoemission spectroscopy

The XPS spectra of vanadium species are shown in Fig. 11 and the binding energies (BE) for all three metals are indicated in Table 3. The deconvolution of the spectra (Fig. 11) allowed identification of the peak at 516.6 eV on the surface of $SbVO_x$(IIa) characteristic of V^{4+} cations [37,38]. This species is not observed on $SbVO_x$(IIb), which can be the reason for the difference in surface properties of both materials. The standard XPS peaks of V $2p_{3/2}$ for V^{5+}, V^{4+} and V^{3+} should be located at 517.2, 515.9 and 515.3 eV, respectively [39]. The BE value of V $2p_{3/2}$ line (517.5 eV) is characteristic of V^{5+} species in V—Sb—O-based systems [40] and is observed on both samples prepared according to methods IIa and IIb. The bulk $VSbO_4$ phase comprises V^{3+} species that must be oxidized at the outermost layer since V species in $VSbO_4$ have a very dynamic redox character [40]. Unsupported oxides show different behaviour, and in addition to V^{5+}, other lower oxidation states ($V^{4+/3+}$) could be found [40], but the spectra shown in Fig. 11 do not indicate the presence of such species, besides the one at 516.6 eV described above. The BE value for Sb $3d_{3/2}$ in the fresh catalyst described in literature is 539.8 eV [41–43]. In our catalysts, this value is a little bit higher (540.2–540.5 eV) and does

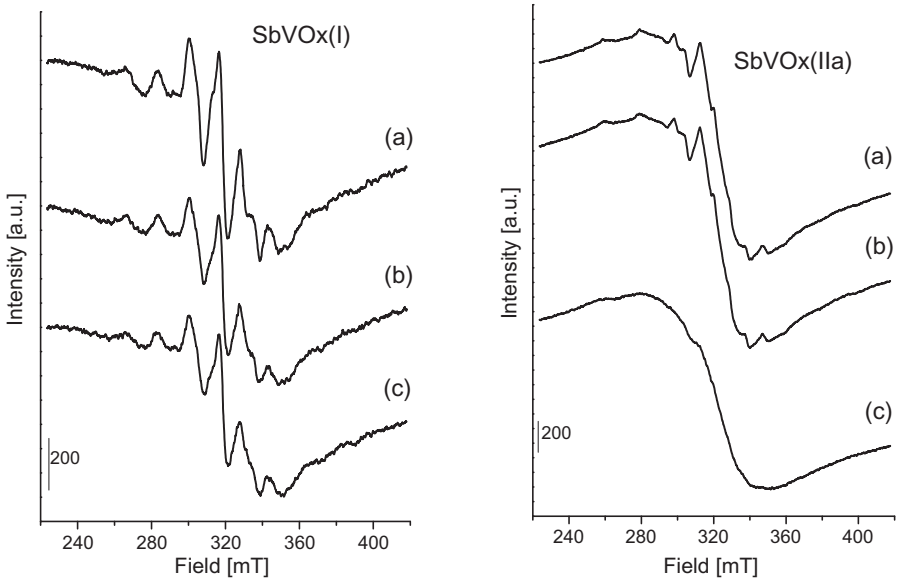

Fig. 9. ESR spectra recorded at RT: (a) sample after evacuation at RT 10 min, (b) after admission of O_2 20 mbar, (c) after heating at 473 K 1 h.

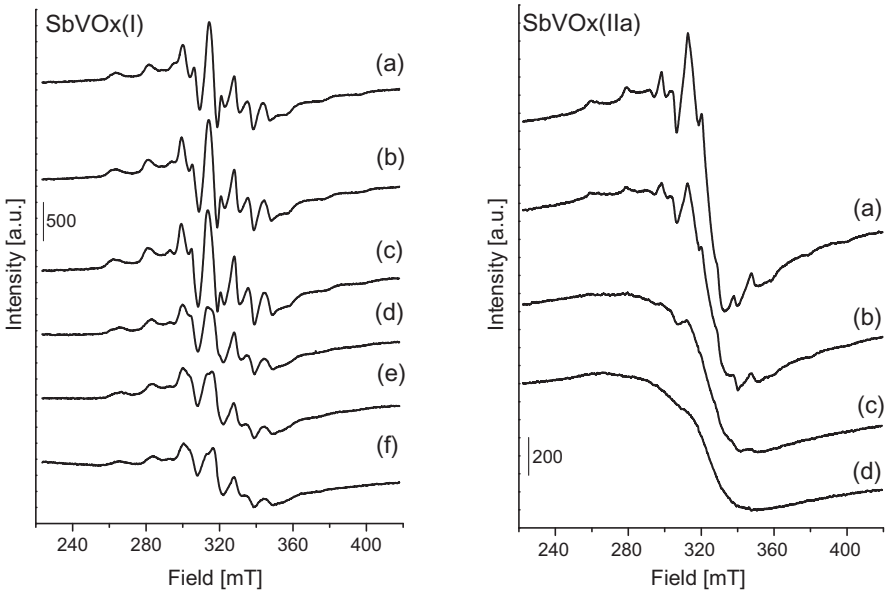

Fig. 10. ESR spectra recorded at RT: (a) fresh sample and after evacuation at: (b) RT 6 h, (c) 373 K 2 h, (d) 473 K 2 h, (e) 573 K 2 h, (f) 673 K.

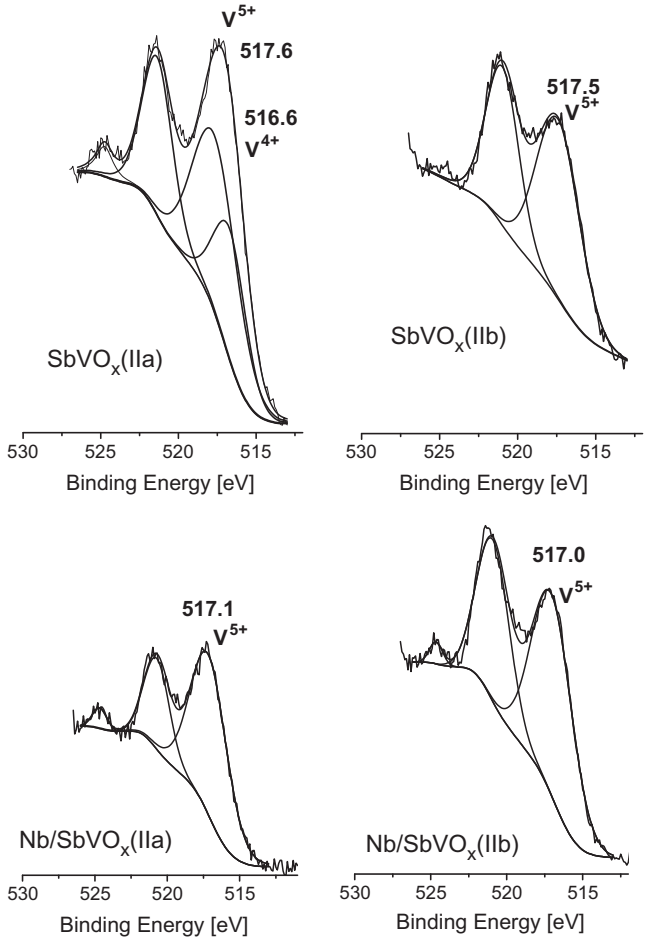

Fig. 11. XPS spectra of vanadium species.

not depend on the niobium loading. On the contrary, the binding energy of V^{5+} cations decreases after niobium loading (Table 3), demonstrating the chemical interaction with niobium species. Identification of the oxidation state of Sb is problematic because

Table 3
XPS results.

Catalyst	Binding energy (eV)		
	V $2p_{3/2}$	Sb $3d_{3/2}$	Nb $3d_{5/2}$-
$SbVO_x$(IIa)	516.6 517.6	540.5	–
$SbVO_x$(IIb)	517.5	540.2	–
Nb/$SbVO_x$(IIa)	517.1	540.4	207.7
Nb/$SbVO_x$(IIb)	517.0	540.2	207.8

the gap between BE of Sb^{3+} and Sb^{5+} is only ~3 eV [44]. An additional complication is that the Sb($3d_{5/2}$) peak almost overlaps that of O(1s) at ~531 eV BE. The binding energies of niobium levels are characteristic of Nb^{5+} species [37], but its BE is a little bit higher (207.7–207.8 eV) than that in bulk niobium(V) oxide (207.1 eV [45]). This phenomenon also supports the occurrence of chemical interaction between niobium and $SbVO_x$ (as indicated above for vanadium species). It is worth noting that in the XPS spectrum of $SbVO_x$(IIa), the V^{4+} signal disappears after niobium loading. This result supports the observations and conclusions from ESR study, indicating the interaction between oxovanadium species and niobium loaded.

The above-described characteristic features of the materials used are responsible for their different surface and catalytic properties.

3.2. Acidity/basicity determination

3.2.1. Pyridine adsorption

Lewis acid (LAS) and BrØnsted acid centres (BAS) were detected in the FT-IR spectra after pyridine adsorption at 373 K and desorption at different temperatures. According to literature, the interaction of pyridine with Lewis acid sites leads to the appearance of bands at ca. 1450 and ~1610 cm^{-1} [46–48]. The intensity of the first one is related to the number of LAS, whereas the position of the second band characterizes the strength of LAS. Adsorption of pyridine on BrØnsted acid sites gives a band at ~1550 cm^{-1} and two other ones in the 1620–1640 cm^{-1} range. Moreover, the bands at 1445 and 1596 cm^{-1}, if appear, originate from pyridine hydrogen bonded to surface hydroxyls [48]. The spectra in Fig. 12 do not indicate a

significant difference between two $SbVO_x$(IIa) and (IIb) samples in the nature of acidity detected by pyridine adsorption. BAS are only slightly indicated by a very broad shoulder, whereas pyridine coordinatively bounded to Lewis acid centres is well characterized by the band at 1445 cm^{-1} and that at ca 1607 cm^{-1}. The position of the latter one is the same for both samples showing the same strength of LAS. It is confirmed by the results of evacuation at different temperatures. Such evacuation systematically decreases the intensity of IR bands from pyridine adsorbed for both samples. However, the calculation of the number of LAS shows a much higher concentration of these centres on the $SbVO_x$(IIa) support at each temperature of desorption applied (Table 4).

3.2.2. Acetonylacetone cyclization

The cyclization of acetonylacetone (AcOAc) was used as a test for acid/base properties. This reaction was proposed by Dessau [49]. The formation of 2,5-dimethylfuran (DMF) occurs at the acidic centres, whereas the production of 3-methyl-2-cyclopentenone (MCP) takes place at the basic centres. On the basis of the MCP/DMF selectivity ratio, the sequence of basicity of the catalysts studied can be proposed. According to literature [49,50], the basicity of the catalyst is demonstrated if MCP/DMF > 1. When MCP/DMF < 1, the catalyst exhibits mainly acidic properties, while MCP/DMF $\sim$ 1 corresponds to the balanced acid–base properties. Table 5 presents the results obtained from this test reaction. All the samples tested exhibit both acidity (DMF production) and basicity (MCP formation) on the surface. The lowest activity is observed for $SbVO_x$(I) sample, whereas all other materials reveal almost the same AcOAc conversion (a little bit higher after niobium loading on the support). However, the selectivity differs significantly depending on the nature of the sample. The highest basicity according to MCP/DMF selectivity ratio is found on $SbVO_x$(IIa) and $SbVO_x$(IIb). This basicity is diminished after niobium loading and the acidity leading to DMF formation slightly dominates for these modified catalysts. Interestingly, acidity dominates on $SbVO_x$(I) support.

3.2.3. 2-Propanol decomposition

The surface properties described above are confirmed by the 2-propanol decomposition performed as a test reaction at the different temperatures. Dehydration of alcohol to propene and/or diisopropyl ether requires acidic centres (Lewis or BrØnsted), whereas the dehydrogenation to acetone occurs on the basic sites [51]. It is noteworthy that ether production requires the presence of pairs of Lewis acid–base centres. Some authors [e.g. 52] have reported that acetone formation takes place on redox centres.

The results obtained within this work are shown in Fig. 13. It is clear that $SbVO_x$(I) exhibits the domination of acidity as follows from almost 100% selectivity to propene. Acetone formed on Lewis basic/redox centres dominates on all other samples when the reaction is carried out at 423 K. With increasing reaction temperature, the selectivity to acetone decreases and that to propene increases. Interestingly, diisopropyl ether is formed on the $SbVO_x$ samples, but not after niobium loading. It is important to point out that diisopropyl ether formation requires the presence of pairs of LAS and LBS (Lewis basic sites). Niobium loading seems to cover the pairs of the required centres. These pairs seems to originate from V=O species [53]. Fig. 13 presents also the selectivity for the same 2-propanol conversion (50%). It is clearly seen that the selectivity to acetone dominates on both $SbVO_x$(IIa) and (IIb) samples, whereas propene is the only product formed on $SbVO_x$(I). Niobium loading causes the significant increase in selectivity to propene, indicating the increase in acidity of the catalysts.

3.3. Methanol oxidation

Table 6 gives the conversion and selectivity for methanol oxidation in steady-state conditions at 423, 473 K (only for $SbVO_x$(I) also at 523 K). The lowest conversion (8% at 473 K) is observed for $SbVO_x$(I), and the main products are dimethyl ether, confirming the significant role of acidic character of the surface, and formaldehyde, indicating the presence of basic/redox sites besides acidic one. Binary oxides prepared by IIa and IIb methods reveal much higher activity and different selectivity in comparison with $SbVO_x$(I). Besides formaldehyde, methyl formate and CO_2 are produced in significant amounts. This phenomenon can be explained by the presence of stronger basic/redox and medium strength acidic centres on the surface. Interestingly, selectivity obtained on both, $SbVO_x$(IIa) and $SbVO_x$(IIb) samples, is very similar. It is in agreement with the observation of similar strength of acidic

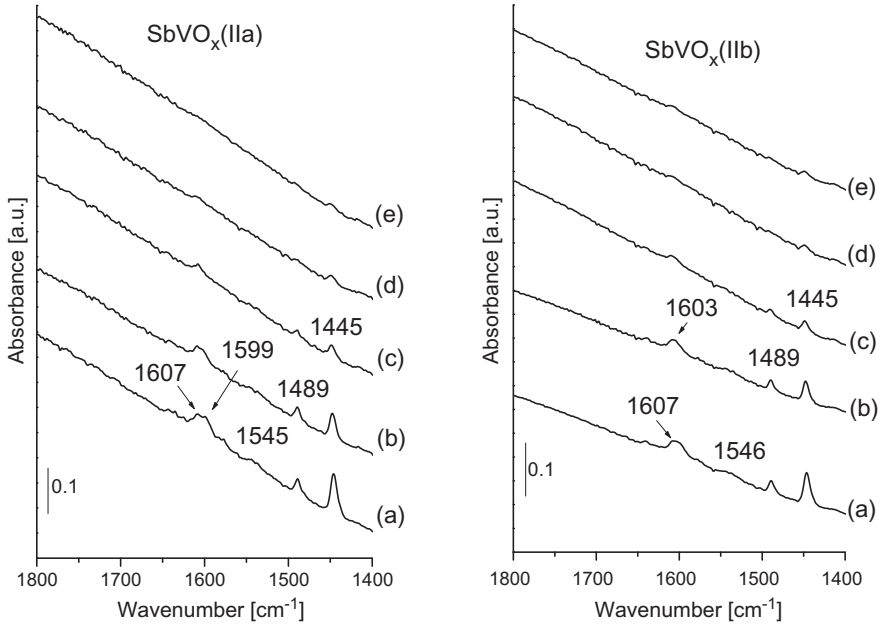

Fig. 12. Infrared spectra: (a) after pyridine adsorption at 373 K and evacuation 5 min and after evacuation 30 min at: (b) 373 K; (c) 373 K; (d) 423 K; (e) 473 K; (e) 523 K.

Table 4
Number of Lewis acid centres calculated from FTIR (a band at 1450 cm^{-1}) spectra after pyridine adsorption and desorption at different temperatures. The extinction coefficient $\varepsilon_{1450} \approx 1.5$ μmol^{-1} from [46,54] was applied.

Temperature of pyridine desorption for 0.5 h (K)	$SbVO_x$(IIa) Number of LAS $\times 10^{16}$	$SbVO_x$(IIb) Number of LAS $\times 10^{16}$
373	15.60	5.89
423	6.95	2.54
473	3.85	0.99
523	2.87	0.93

Table 5
The results of acetonylacetone (AcOAc) cyclization at 623 K.

Catalyst	AcOAc conv. (%)	Selectivity (%)		MCP/DMF
		DMF[a]	MCP[a]	
$SbVO_x$(I)	8	71	29	0.408
$SbVO_x$(IIa)	13	32	68	2.125
$SbVO_x$(IIb)	12	19	81	4.263
Nb/$SbVO_x$(IIa)	14	55	45	0.818
Nb/$SbVO_x$(IIb)	14	54	46	0.851

[a] MCP – 3-methyl-2-cyclopentenone; DMF – 2.5-dimethylfuran.

centres deduced from pyridine adsorption and desorption and similar production of acetone in 2-propanol dehydrogenation observed for both samples. Although the selectivity in methanol oxidation carried out on both samples prepared with the use of the template is almost the same, the conversion of methanol is significantly different. The activity of $SbVO_x$(IIa) is much higher than that of $SbVO_x$(IIb). It is in line with the number of LAS on the catalyst surface supporting the mechanism of methanol oxidation in which the first step of the reaction involves the dissociative adsorption of methanol molecules with the formation of methoxy species on Lewis acid centres [1,4,54]. One has also to consider the role of different surface areas of both samples. For the expression of methanol conversion on 1 m^2 of the surface (Table 6), the activity of $SbVO_x$(IIa) is slightly higher than that of $SbVO_x$(IIb).

Niobium loading on both binary oxides, prepared with the use of the template, leads to a slight increase in methanol conversion and to a total change in selectivity. Significant amounts of DMM are present among the reaction products. Moreover, the selectivity to FA decreases at 423 K and increases at 473 K after niobium loading on $SbVO_x$. Such behaviour can be explained by the change in the acidic strength resulting from Nb—V interaction and by decrease in the amount of active oxygen on the $SbVO_x$ surface after Nb loading. The occurrence of Nb—V interaction was indicated by

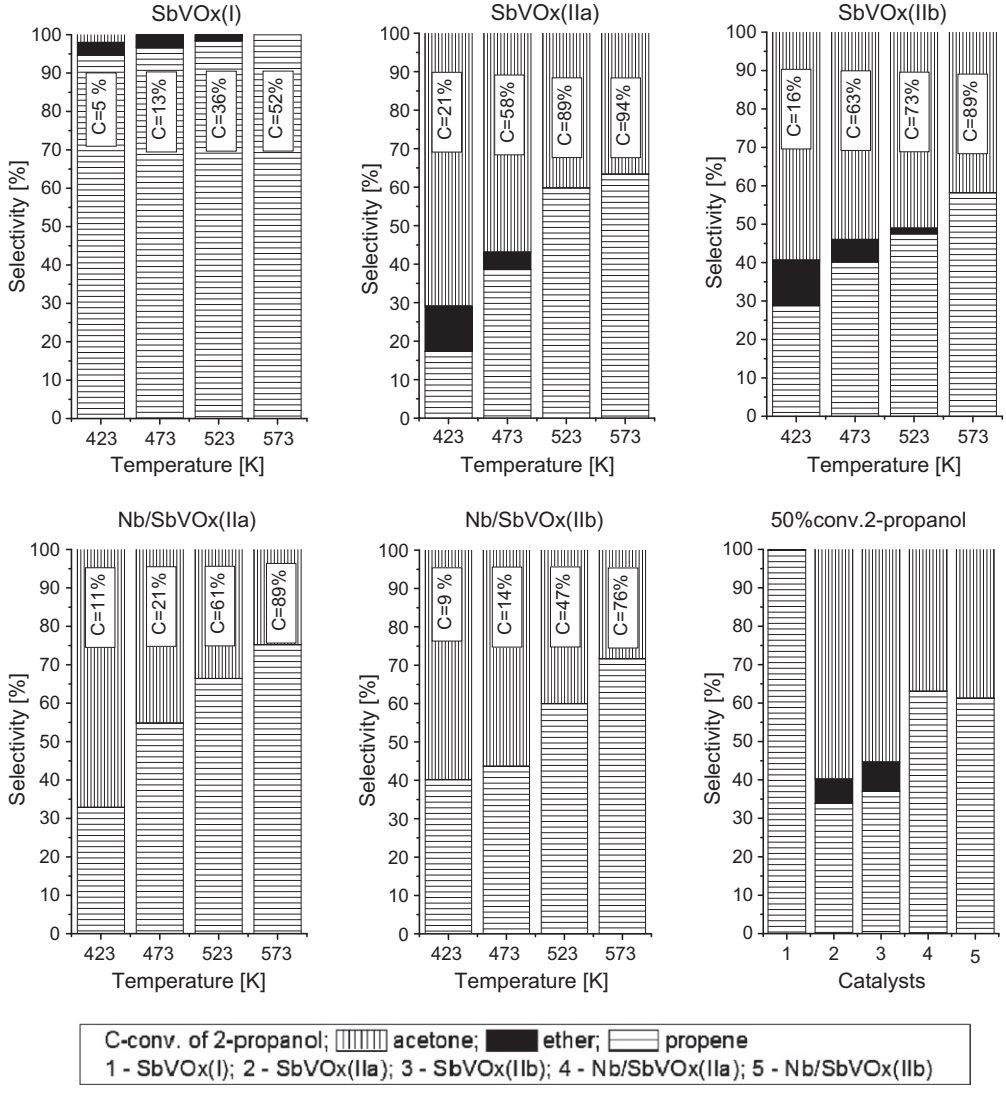

Fig. 13. The results of 2-propanol decomposition at 423, 473, 523, 573 K and selectivity for 50% of 2-propanol conversion on all catalysts.

Table 6
The results of methanol oxidation (40 cm^3 min^{-1} Ar/O_2/MeOH (88/8/4 mol%) flow used as a reactant mixture).

Catalyst	Temp. (K)	CH_3OH conv. (mmol/m^2)	CH_3OH conv. (%)	Selectivity (%)				
				HCHO	CH_3OCH_3	$HCOOCH_3$	$(CH_3O)_2CH_2$	CO_2
$SbVO_x$(I)	473	0.057	8	40	46	3	11	Traces
	523	0.243	34	50	43	4	3	–
$SbVO_x$(IIa)	423	0.168	38	57	1.5	28	1	12.5
	473	0.261	59	33	1	15	2	49
$SbVO_x$(IIb)	423	0.142	26	56	1	26	4	13
	473	0.251	46	30	1	29	3	37
$Nb/SbVO_x$(IIa)	423	0.402	39	33	1	5	36	25
	473	0.640	62	69	1	2	15	13
$Nb/SbVO_x$(IIb)	423	0.243	34	27	1	4	39	29
	473	0.421	59	59	1	1	21	18

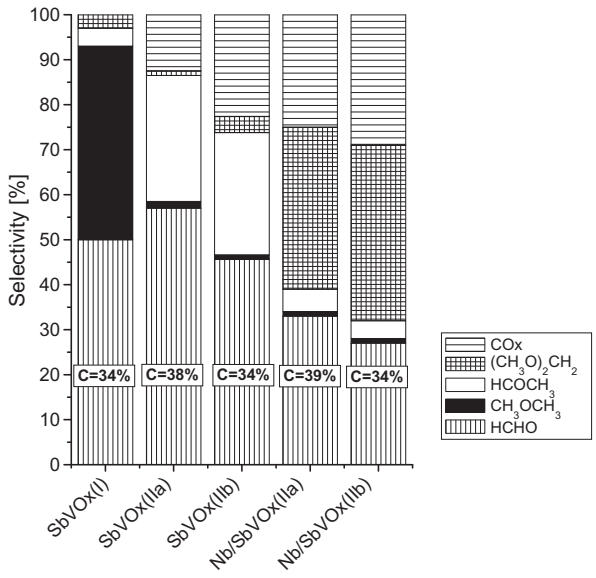

Fig. 14. Selectivity in methanol oxidation (40 cm^3 min^{-1} Ar/O_2/MeOH (88/8/4 mol%) flow used as a reactant mixture) for the conversion (C) in the range of 34–39%.

the results of XPS, UV–vis, ESR studies. It leads to more effective reaction of CH_2O adsorbed with methanol molecules towards DMM which is a competitive process to the oxidation of CH_2O to CHOOH and CO_2 (Fig. 1). Stronger chemisorption of FA makes further interaction with the next methanol molecules much easier and DMM is easier formed. However, the increase in the reaction temperature to 473 K facilitates desorption of formaldehyde due to the temperature effect. Therefore, the selectivity to DMM is lower at this temperature and that to FA is higher.

The reaction selectivity for methanol conversion in the range 34–39% is illustrated in Fig. 14. It is well visible that contrary to $SbVO_x$(I), $SbVO_x$(IIa) and $SbVO_x$(IIb) lead to generation of significant amounts of CO_2, which requires the presence of oxygen playing the role of basic/redox centre. The decrease in FA selectivity results in the increase of CO_2 formation. After niobium loading, the highest changes in selectivity are noted for DMM and MF. One observes the significant increase in DMM production and decrease in MF selectivity. The FT-IR spectra of the catalysts after methanol oxidation show some small differences (Fig. 15). Although no shift of the original frequencies is detected, it is noticeable that the intensity of the band at ~1007 cm^{-1} decreases, whereas the intensities of the bands at 540, 665, and 735 cm^{-1} increase. It suggests some rearrangement of the catalyst crystalline phases, which is confirmed by the ESR spectrum of the used catalyst, in which the hyperfine structure characteristic of the isolated VO^{2+} ions disappeared (Fig. 15).

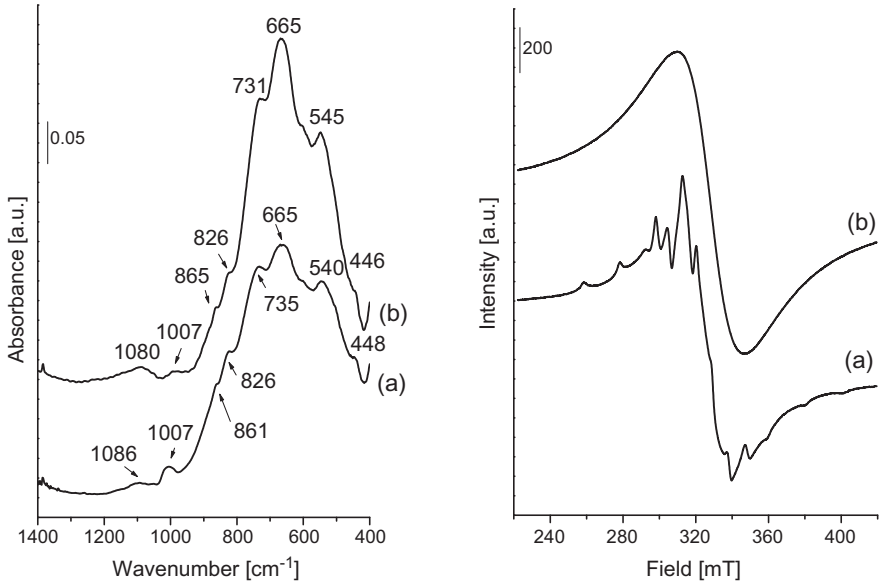

Fig. 15. FTIR and ESR spectra of $SbVO_x$(IIa) (a) fresh and (b) catalyst after methanol oxidation.

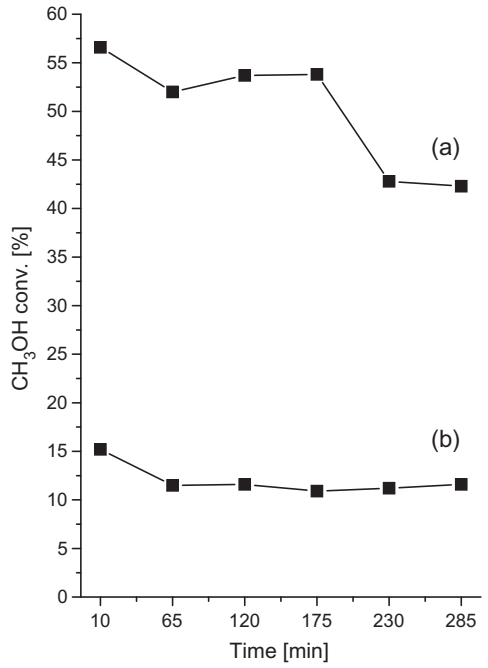

Fig. 16. Conversion of methanol at 473 K on $SbVO_x$(IIa): (a) before pyridine admission and (b) after poisoning with pyridine.

For better understanding of the role of acidic centres, the oxidation of methanol was performed on $SbVO_x$(IIa) after the catalyst poisoning with pyridine adsorption. A portion of 1 μl of pyridine was injected into the reactor at 473 K in the flow of argon and after 15 min of Ar flowing, the reaction mixture containing methanol and oxygen was passed. The results are shown in Fig. 16. A considerable decrease in the methanol conversion after pyridine adsorption is evident. At this temperature, pyridine blocks stronger LAS and therefore, the weaker acidic centres can interact with the reagents giving rise to methanol conversion.

As follows from the mechanism of methanol oxidation, both acidic centres and surface oxygen are important for the activity and selectivity of this process. To get a deeper insight into the role of surface oxygen, the reaction on $SbVO_x$(IIb) was performed at 473 K without the presence of oxygen in the reagents mixture. The results are shown in Table 7. Methanol undergoes oxidative dehydrogenation towards FA when the oxygen free mixture is passed through the reactor. The activity is low and decreases with the time on stream. The participation of surface oxygen in FA formation is clear from this experiment. The admission of oxygen into the reagents mixture considerably increases the conversion and changes the selectivity, in particular the selectivity to FA. Interestingly, $Nb/SbVO_x$(IIb) was inactive in the reaction of oxygen free mixture. It suggests that the active oxygen on the surface of $SbVO_x$ interacts with niobium species.

To establish the conditions ensuring the highest DMM generation, the methanol oxidation reaction was performed in different conditions. Generally, the idea was to increase the amount of methanol in the reagents mixture, close to the stoichiometry needed for the formation of DMM. It was realized by an increase in the methanol amount in the mixture of gases. The results are summarized in Table 8. The use of methanol excess or the 1:1 O_2: MeOH ratio allows us to obtain 100% selectivity to DMM at 423 K.

4. Discussion

It is known that because of the influence of preparation route on the structural and phase composition, the catalytic behaviour of binary oxides ($SbVO_x$) considerably depends on the method of synthesis [55]. In this study, we prepared $SbVO_x$ oxides with the use of the template (Pluronic 123) to increase the surface area and porosity of the material. These binary oxides were used as catalysts and as supports for niobium species loaded. The main focus was on the application of the catalysts prepared in the low temperature oxidation of methanol. The use of a template during the synthesis increases not only the surface area and pore volume of the final material if compared to those of the binary oxide prepared without the template, but also changes the phase composition of $SbVO_x$ system. The same initial amounts of V and Sb sources used for all the synthesis procedures give rise to different phase compositions depending on the synthesis method. All samples contain rutile $SbVO_4$ phase but in the samples obtained by the template-assisted preparation, some amounts of α-Sb_2O_4 phase were also present as indicated by the FTIR spectra (the band at ~450 cm^{-1}) and XRD patterns (Fig. 5). In contrast, some additional V_2O_5 phase was detected (XRD, UV–vis) in $SbVO_x$(I) sample. The appearance of these phases has an impact on the catalytic activity of the surface. Sb_2O_4 is a p-type semiconductor [56], and therefore, the electron transfer can occur from vanadium species in $SbVO_x$ to Sb_2O_4 at the interface of these two phases. Then oxygen vacancies can be formed and promote the chemisorption of O_2. The oxygen ion O^{2-} spills over the interface between Sb_2O_4 and $SbVO_x$. Therefore,

Table 7
Methanol conversion on $SbVO_x$(IIb) at 473 K without oxygen (for 120 min) and in the presence of oxygen.

Reaction conditions	Time (min)	CH_3OH conv. (%)	Selectivity (%)				
			HCHO	CH_3OCH_3	$HCOOCH_3$	$(CH_3O)_2CH_2$	CO_2
MeOH + argon	65	12	95	0	0	5	0
	120	10	95	0	0	5	0
MeOH + O_2 + argon	230	40	38	1	6	15	40
	285	43	35	1	5	12	47

Table 8
Methanol oxidation on $SbVO_x$(IIa) at different reaction conditions.

Reaction conditions	Reaction temp., (K)	CH_3OH conv. (%)	Selectivity (%)				
			HCHO	CH_3OCH_3	$HCOOCH_3$	$(CH_3O)_2CH_2$	CO_2
$Ar/O_2/CH_3OH$ (88/4/8 mol%) O_2/MeOH = 0.5	423	3	–	–	–	100	–
	473	7	67	Traces	–	33	–
$Ar/O_2/CH_3OH$ (92/4/4 mol%) O_2/MeOH = 1	423	12	–	–	–	100	–
	473	16	61	1	6	32	–

the partially reduced vanadium species can be reoxidized and contribute to the increase in the catalytic activity in methanol oxidation as established for H_2S oxidation on V_2O_5 doped with Sb_2O_4 [39]. The promoting effect of α-Sb_2O_4 can be the reason for a considerably higher methanol conversion on both $SbVO_x$(IIa) and (IIb) samples compared with the activity achieved on $SbVO_x$(I). Moreover, as concluded from ESR spectra, $SbVO_x$(I) contains more saturated VO^{2+} isolated species than both materials synthesised with the use of template (method II). Less saturated vanadyl ions are more active in the chemisorption of reagents. Relation of the activity to surface area of $SbVO_x$ samples prepared by method I and II confirms the significant higher methanol conversion on samples IIa and IIb than on I material.

A comparison of the percentage of methanol conversion over $SbVO_x$(IIa) and (IIb) samples has shown much higher activity of the first catalyst. Therefore, the activity cannot be related only to the promoting role of α-Sb_2O_4 present on both catalysts, but also to the other features. Firstly, the different surface areas of both materials should be considered. The activity calculated per 1 m^2 of the catalyst surface indicated that more methanol molecules are converted on 1 m^2 of $SbVO_x$(IIa) than on 1 m^2 of $SbVO_x$(IIb). Thus, the higher surface area of $SbVO_x$(IIa) is not the only feature which can determine its higher activity. Reducible vanadium VO^{2+} species have to play an important role in oxidation of methanol. They are different in (IIa) and (IIb) samples. According to ESR results, isolated VO^{2+} (V=O) paramagnetic species were present on $SbVO_x$(IIb), whereas higher concentration of these cations forming dimmers was found on $SbVO_x$(IIa). V=O plays a role of pair of Lewis acidic and basic centres. Pyridine adsorption and desorption experiments pointed out a higher concentration of LAS on $SbVO_x$(IIa) than on $SbVO_x$(IIb), which is in agreement with the ESR results and activity in acid–base catalyzed reactions, i.e. 2-propanol decomposition and AcOAc cyclization. The presence and concentration of Lewis acid sites are important, because in the first step of oxidation of methanol, the methoxy species are formed on these centres [e.g. 1,4]. The role of these acid centres was confirmed by a significant drop in methanol conversion after pyridine adsorption on LAS.

In oxidation of methanol not only acidic centres are involved but also redox/basic sites. To check whether active oxygen is present on the catalyst surface or it is chemisorbed from the gas phase, the methanol transformation without the use of oxygen in the gas mixture was performed. It was clear that $SbVO_x$(IIb) catalyst activates the transformation of methanol to formaldehyde without gas oxygen, indicating the use of the surface oxygen for this purpose. After a decrease in the activity with time on stream, a mixture of methanol and oxygen was passed through the catalyst bed and the activity increased and selectivity came to that observed in the standard oxidation of methanol (Table 7). These results point out that the surface oxygen is used for the oxidation of methanol to formaldehyde, and the catalyst surface is reoxidised with gaseous oxygen.

The question arises which oxygen on the catalyst surface is active in the oxidation of methanol. The answer to this question comes from a detailed study of $SbVO_x$ modified with niobium species. It was shown that niobium (in the form of Nb_2O_5) loading on $SbVO_x$(IIa) considerably changes the surface properties of the catalyst, namely: (i) decreases the concentration of V^{4+} as indicated by the XPS spectra, (ii) removes the presence of hyperfine structure from the ESR lines assigned to VO^{2+} species, (iii) decreases binding energy of V^{5+} cations, (iv) eliminates the formation of diisopropyl ether (requiring the presence of LAS and LBS) in dehydration of 2-propanol, (v) makes the catalyst inactive in the oxidative dehydration of methanol to formaldehyde without the use of gas oxygen. As follows from the above, it is the oxygen from V=O that is active in methanol oxidation. Niobium loaded blocks the access to the active oxygen. Such behaviour of niobium species changes the selectivity of the reaction. According to the reaction scheme shown in Fig. 1, a competition takes place between the reaction of chemisorbed FA with oxygen and with other methanol molecules, to DMM production. On niobium-modified catalysts, significant amount of DMM is formed, showing the preference of the interaction of chemisorbed FA with methanol not with oxygen. By increasing the concentration of methanol in the reagent mixture, one can obtain 100% selectivity to DMM at 423 K even over the catalysts without niobium species.

Finally, the reason for the difference in surface properties between $SbVO_x$(IIa) and (IIb) should be discussed. Both samples were synthesized in the presence of template – the precursors of V and Sb were added to the solution of Pluronic 123. However, when both metal sources were admitted from separate flasks, the stirred solution containing all components was not fully homogeneous and therefore, the concentration of vanadium species located on the particle surface became higher ($SbVO_x$(IIa)) than when both metal sources were mixed before addition to the Pluronic 123 solution ($SbVO_x$(IIb)). This behaviour determines the catalytic activity and selectivity of the catalysts.

5. Conclusions

The structure and phase composition – activity and selectivity dependence in the oxidation of methanol is evidenced within this study performed on $SbVO_x$ catalysts also modified with niobium species. All the catalysts used contain rutile binary oxides $SbVO_4$ in which reducible oxovanadium species play a role on active centres in the oxidation of methanol. The nucleophilic oxygen from V=O species plays a crucial role in the oxidation of methanol. Niobium oxide loading on $SbVO_x$ support blocks the active oxygen species and changes the selectivity in methanol oxidation towards DMM formation. Template-assisted synthesis creates unsaturated VO^{2+} species (contrary to the stable saturated species in $SbVO_x$(I) sample) active in the chemisorption of reagents and their further transformation. The presence of α-Sb_2O_4 phase formed in the template-assisted synthesis promotes the electron transfer from oxovanadium species enhancing the activity in methanol oxidation. The presented results indicate that using different procedures of synthesis of binary $SbVO_x$ oxides and their modification with niobium species, it is possible to obtain catalysts useful for selective production of desired products (FA or MF or DMM).

Acknowledgment

Polish Ministry of Science and Higher Education (Grant No N 204 016439) is acknowledged for a financial support.

References

[1] J.M. Tatibouet, Appl. Catal. A: Gen. 148 (1997) 213.
[2] C.H. Bartholomew, R.J. Farrauto, Fundamentals of Industrial Catalytic Processes, John Wiley & Sons, Inc., 2005. pp. 586–597.
[3] L. Burcham, I.E. Wachs, Catal. Today 49 (1999) 467.
[4] G. Busca, A.S. Elmi, P. Forzatti, J. Phys. Chem. 91 (1987) 5263.
[5] G. Centi, S. Perathoner, Selective oxidation – industrial, in: I. Horvath (Ed.), Encyclopedia of Catalysis, Wiley-Interscience, Hoboken, NJ, 2003, p. 239.
[6] X. Gao, I.E. Wachs, M.S. Wong, J.Y. Ying, J. Catal. 203 (2001) 18.
[7] B.M. Weckhuysen, D.E. Keller, Catal. Today 78 (2003) 25.
[8] K. Routray, W. Zhou, C.J. Kiely, I.E. Wachs, ACS Catal. 1 (2011) 54.
[9] I.E. Wachs, Appl. Catal. A: Gen. 391 (2011) 36.
[10] Q.D. Zhang, Y.S. Tang, C.H. Yang, Y.Z. Hang, J. Mol. Catal. A 263 (2007) 149.
[11] X. Lu, Z. Qin, M. Dong, H. Zhu, G. Wang, Y. Zhao, W. Fan, J. Wang, Fuel 90 (2011) 1335.
[12] H. Zhao, S. Bennici, J. Shen, A. Auroux, J. Catal. 272 (2010) 176.
[13] O.A. Nikonova, M. Capron, G. Fang, J. Faye, A.S. Mamede, L. Jalowiecki-Duhamel, F. Dumeignil, G.A. Seisenbaeva, J. Catal. 279 (2011) 310.
[14] H. Liu, E. Iglesia, J. Catal. 223 (2004) 161.

[15] J. Gornay, X. Sécordel, B. de Ménorval, S. Cristol, P. Fongarland, M. Capron, L. Duhamel, E. Payen, J.-L. Dubois, F. Dumeignil, Green Chem. 12 (2010) 1722.
[16] H. Golinska, P. Decyk, M. Ziolek, Catal. Today 169 (2011) 242.
[17] H. Zhang, Z. Liu, Z. Feng, C. Li, J. Catal. 260 (2008) 295.
[18] M.O. Guerrero-Pérez, M.A. Vicente, J.L.G. Fierro, M.A. Bañares, Chem. Matter 19 (2007) 6621.
[19] M.D. Allen, S. Poulston, E.G. Bithell, M.J. Goringe, M. Bowker, J. Catal. 163 (1996) 204.
[20] D. Hong, V.P. Vislovskiy, Y. Hwang, S.H. Jhung, J.S. Chang, Catal. Today 131 (2008) 140.
[21] G. Catana, R. Ramachandra Rao, B.M. Weckhuysen, Pascal Van Der Voort, E. Vansant, R.A. Schoonheydt, J. Phys. Chem. B 102 (1998) 8005.
[22] M. Nashimura, K. Asakura, Y. Iwasawa, J. Chem. Soc. Chem. Commun. 15 (1986) 1660.
[23] M. Trejda, A. Wojtaszek, A. Floch, R. Wojcieszak, E.M. Gaigneaux, M. Ziolek, Catal. Today 158 (2010) 170.
[24] H. Matsumura, K. Okumura, T. Shimamura, N. Ikenaga, T. Miyake, T. Suzuki, J. Mol. Catal. A 250 (2006) 122.
[25] J. Nillson, A. Landa-Canovas, S. Hansen, A. Andersson, Catal. Today 33 (1997) 97.
[26] C. Popa, M.V. Ganduglia-Pirovano, J. Sauer, J. Phys. Chem. C 115 (2011) 7399.
[27] M. Baron, H. Abbott, O. Bondarchuk, D. Stacchiola, A. Uhl, S. Shaikhutdinov, H.J. Freund, C. Popa, M.V. Ganduglia-Pirovano, J. Sauer, Angew. Chem. Int. Ed. 48 (2009) 8006.
[28] M. Bowker, C.R. Bicknell, P. Kerwin, Appl. Catal. A: Gen. 136 (1996) 205.
[29] M. Baltes, K. Cassiers, P. Van Der Voort, B.M. Weckhuysen, R.A. Schoonheydt, E.F. Vansant, J. Catal. 197 (2001) 160.
[30] Z. Luan, J. Xu, H. He, J. Klinowski, L. Kevan, J. Phys. Chem. 100 (1996) 19595.
[31] M. Ziolek, I. Nowak, B. Kilos, I. Sobczak, P. Decyk, M. Trejda, J.C. Volta, J. Phys. Chem. Solids 65 (2004) 571.
[32] J. Typek, E. Filipek, M. Maryniak, N. Guskos, Mater. Sci. Poland 23 (2005) 1047.
[33] J. Typek, N. Guskos, D. Buchowski, M. Wabia, E. Filipek, Radiat. Effects Defects Solids 157 (2002) 1093.
[34] G. Centi, S. Perathoner, F. Trifiro, J. Phys. Chem. 96 (1992) 2617.
[35] M.C. Paganini, L. Dall Aqua, E. Giamello, L. Lietti, P. Forzatti, G. Busca, J. Catal. 166 (1997) 95.
[36] B.A. Goodman, J.B. Raynor, Adv. Chem. Radiochem. 13 (1970) 135.
[37] R. Lopez-Medina, J.L.G. Fierro, M.O. Guerrero-Perez, M.A. Banares, Appl. Catal. A: Gen. 375 (2010) 55.
[38] M.O. Guerrero-Perez, M.C. Herrera, I. Malpartida, M.A. Larrubia, L.J. Alemany, Catal. Today 118 (2006) 360.
[39] D.W. Park, B.K. Park, D.K. Park, H.Ch. Woo, Appl. Catal. A: Gen. 223 (2002) 215.
[40] M.O. Guerrero-Perez, M.A. Pena, J.L.G. Fierro, M.A. Banares, Ind. Eng. Chem. Res. 45 (2006) 4537.
[41] S. Larrondo, B. Irigoyen, G. Baronetti, N. Amadeo, Appl. Catal. A: Gen. 250 (2003) 279.
[42] T. Shishido, T. Konishi, I. Matsuura, Y. Wang, K. Takaki, K. Takehira, Catal. Today 71 (2001) 77.
[43] E.K. Novakova, J.C. Vedrine, E.G. Derouane, J. Catal. 211 (2002) 235.
[44] C.D. Wagner, Discuss. Faraday Soc. 60 (1975) 291.
[45] M. Ziolek, P. Decyk, I. Sobczak, M. Trejda, J. Florek, H. Golinska, W. Klimas, A. Wojtaszek, Appl. Catal. A: Gen. 391 (2011) 194.
[46] S. Khabtou, T. Chevreau, J.C. Lavalley, Microporous Mater. 3 (1994) 133.
[47] E.P. Parry, J. Catal. 2 (1963) 371.
[48] B. Chakraborty, B. Viswanathan, Catal. Today 49 (1999) 253.
[49] R.M. Dessau, Zeolites 10 (1990) 205.
[50] J.J. Alcaraz, B.J. Arena, R.D. Gillespie, J.S. Holmgren, Catal. Today 43 (1998) 89.
[51] A. Gervasini, J. Fenyvesi, A. Auroux, Catal. Lett. 43 (1997) 219.
[52] C. Lahousse, J. Bachelier, J.C. Lavalley, H. Lauron-Pernot, A.M. Le Govic, J. Mol. Catal. 87 (1994) 329.
[53] M. Trejda, M. Ziolek, Y. Millot, K. Chalupka, M. Che, S. Dzwigaj, J. Catal. 281 (2011) 169.
[54] M. Ziolek, I. Nowak, J.C. Lavalley, Catal. Lett. 45 (1997) 259.
[55] G. Centi, S. Perathoner, F. Trifiro, Appl. Catal. A Gen. 157 (1997) 143.
[56] G.W. Godin, C.C. McCain, E.A. Porter, in: Proceedings of the 4th International Congress on Catalysis, vol. 1, 1997, p. 271.